Strain Analysis of Archean, Metasedimentary Rocks in the Virginia Horn, Northeastern Minnesota

Robert Holder
Undergraduate Thesis under James "Jim" Welsh
Gustavus Adolphus College
May 2012

Abstract

The "Virginia Horn" is a prominent anticline/syncline pair in Proterozoic rocks of the Biwabik Iron Formation, northeastern Minnesota, that exposes Neoarchean metavolcanic and metasedimentary basement rocks in the anticlinal core. Three deformation events have been identified: D_1, D_2, and D_3. This study uses the *Rf/Φ* strain analysis method on lithic and quartz clasts from low-grade metasedimentary rocks to quantify their deformational history. The lithic clasts record moderately intense, plane to slightly constrictive strain, while the quartz clasts record milder, more precise plane strain. This study attributes the discrepancy in strain values to be the result of a ductility contrast between the two clast types, however it could also be caused by non-ellipsoidal clasts and/or randomness associated with the study's small sample size. The majority of the strain in these rocks appears to come from D_2, due to the nearly vertical long axes of strain and corresponding field evidence.

Acknowledgements

I would like to thank Jim Welsh for providing me with the opportunity to undertake this project, my initial resources and ideas, and slowing me down when I tried to do too much at once. I would also like to thank Laura Triplett and Julie Barley for helping me with the writing process and keeping a necessarily strict timeline to accomplish this study on a restricted schedule.

Table of Contents

Introduction

The "Virginia Horn" refers to the prominent bend in the outcrop pattern of Paleoproterozoic rocks of the Mesabi Iron Range in northeastern Minnesota (Fig. 1), that represents a northeasterly-trending anticline/syncline pair in the Biwabik Iron Formation. Supracrustal Neoarchean metamorphic basement rocks are exposed in the core of the anticline. These sequences are separated from the overlying Paleoproterozoic rocks by a significant nonconformity and from other rocks of similar ages by the Laurentian Fault (Fig. 1, Fig. 2) (Jirsa & Boerboom, 2003, Welsh et al., 1991). This strain analysis examines samples of greywacke-slate from within the Virginia Horn in order to see how the internal fabric of the rocks compares to the recognized deformation events, providing a better understanding of the region's tectonic history.

Geologic Setting

The Archean rocks of the area are considered to be an extension of the Wawa Subprovince of the Superior Province (Jirsa and Boerboom, 2003), and are separated from similar rocks in the Vermillion District to the north by the Giants Range Batholith (Fig 1). The Archean rocks have been separated into three sequences (Jirsa and Boerboom, 2003) (Fig. 2):

- the Minntac Sequence: a sequence of mid amphibolite-grade metavolcanic and metasedimentary rocks which were intruded by the Giants Range Batholith to the north.
- the Mud Lake Sequence: a sequence of metavolcanic and metasedimentary rocks similar to the Minntac sequence, however this sequence exhibits only prehnite-pumellyite to low-grade greenschist facies metamorphism. The rocks contain rhythmic, graded beds of various thickness and are composed almost totally of felsic-intermediate volcanic detritus which has been interpreted as a proximal, submarine-fan environment from nearby volcanic centers to the east (Welsh et al., 1991, Levy, 1991, Jirsa & Boerboom, 2003). The Mud Lake Sequence is in contact with the Minntac Sequence and the Giants Range Batholith to the north along the east-west trending Laurentian Fault and also contains a few small felsic intrusives, such as the Viking Porphyry, which have been the target of gold exploration.
- the Midway Sequence: a metasedimentary sequence of conglomerate/lithic sandstone protolith, which lies uncomformably above the Mud Lake Sequence.

Jirsa and Boerboom (2003) have identified three periods of deformation in these rocks, referred to in relative chronological order as D_1, D_2, and D_3. Exact age constraints have not been determined. D_1 resulted in upright folding about sub-horizontal axes, including the southwest-trending "Mud Lake Syncline," soft-sediment deformation, and "complex faulting" (Jirsa and Boerboom 2003, p 11). D_2 involved regional horizontal shortening along with minor folding. S_2, a metamorphic cleavage present in the Mud Lake and Midway sequences, is associated with D_2. D_3 consists of open folds about sub-horizontal axes which trend roughly parallel to the axis of the Virginia Horn. In addition to the folding events, J. Welsh (Welsh, 1989, Welsh et al., 1991) has identified a sinistral, strike-slip, fault/shear complex that cuts across the Archean units and also parallels the Virginia Horn's axis. Displacement along this system has been accommodated primarily by the Pike River Fault in the northern part of the area, while to the south the fault splays into a

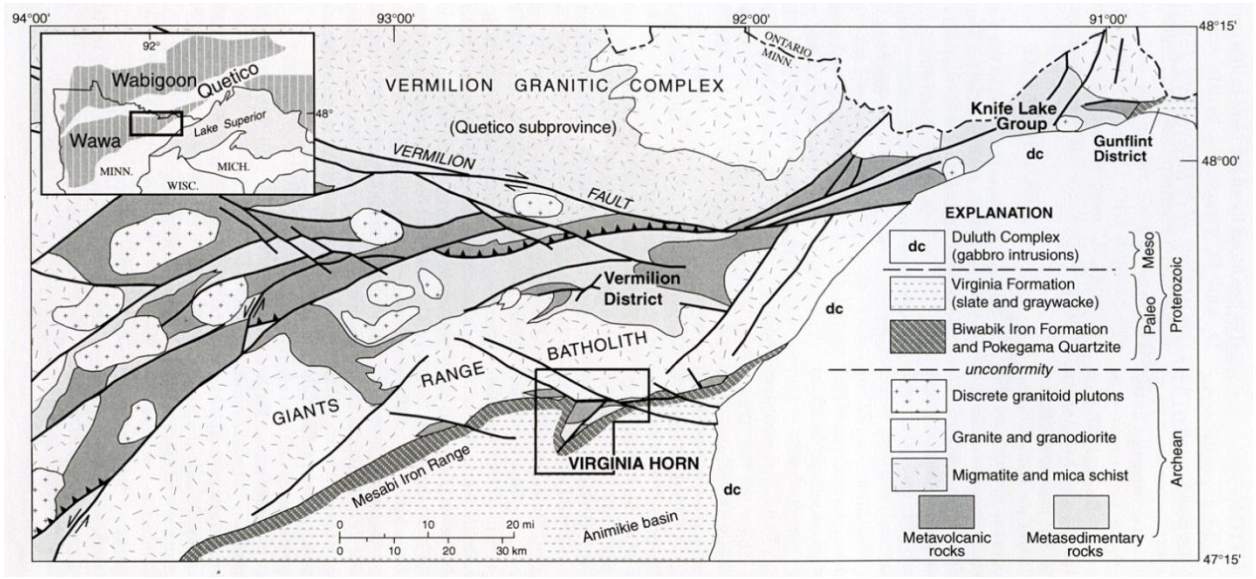

Figure 1. Regional geology of northeastern Minnesota and the relationship between the Virginia horn and similar rocks of the Wawa Province (Morey and Jirsa, 2003).

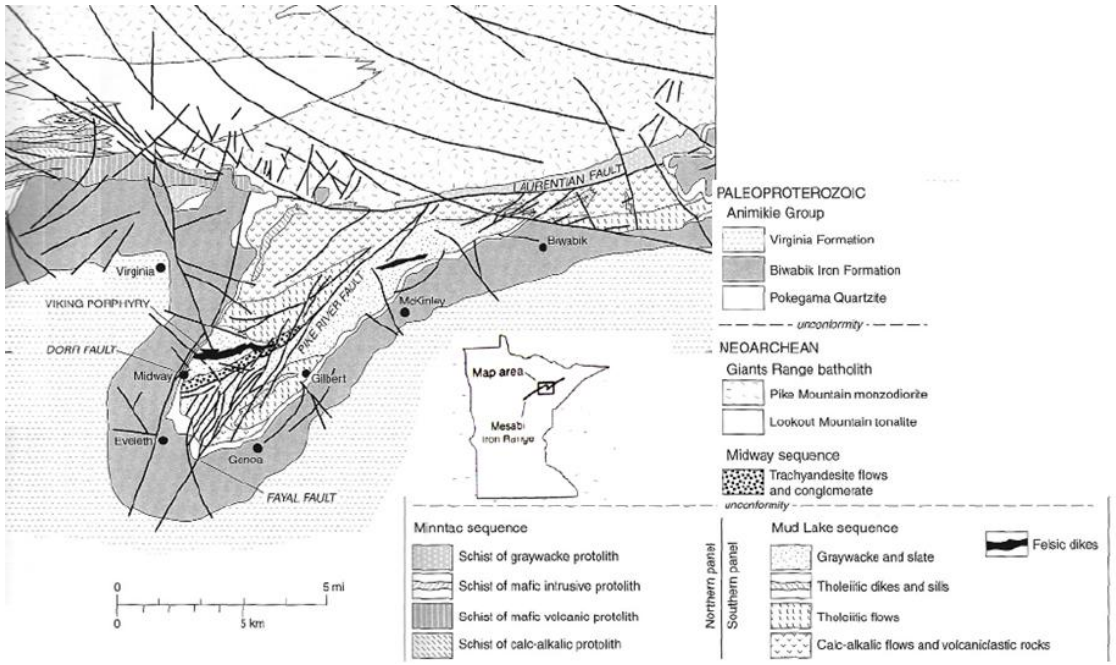

Figure 2. Geologic Map of the Virginia Horn (Jirsa & Boerboom, 2003) and its location in Minnesota (Morey and Jirsa, 2003).

complex system of narrow faults (Fig 2). J. Welsh (1989, personal communication, 2012) has suggested that these structures, together with the Fayal Fault to the south (Fig 2), might represent a strike-slip duplex. Jirsa and Boerboom (2003) consider the development of the splayed faulting between the Pike River Fault and the Fayal Fault to have formed during D_3, but do not provide conclusive interpretation. Welsh (personal communication, 2012) has suggested that they were caused by reactivation of the Pike River and Fayal Faults – possibly during the Penokean Orogeny of the Early Proterozoic.

Previous Work

Morey and Jirsa (2003) report on the history of mapping and exploration in the region. Geologic mapping and structural work in the Virginia Horn has been carried out since the 1800's due to mineral interests, specifically iron and gold. More recent, comprehensive field work and mapping has been carried out by Welsh (Welsh et al., 1989, Welsh et al., 1991); Levy (1991); Jirsa, Boerboom, and Morey (1998); Jirsa and Boerboom (2003); and Jirsa, Chandler, and Lively (2005).

Previous strain analysis work on the Mud Lake sequence was carried out by Christensen (2009). Christensen measured the strain recorded in quartz grains from oriented samples collected from the greywacke-slate unit of the Mud Lake Sequence, by J.Welsh. This research aimed to determine the strain recorded by lithic grains in the same set of oriented samples using the R_f/Φ technique.

Methods

Sample Collection

Twenty samples from the greywacke-slates of the Mud Lake sequence were collected by Jim Welsh during previous fieldwork. Each sample was field oriented (strike and dip were measured and marked on each sample) with respect to the S_2 metamorphic cleavage in order to facilitate the strain analysis. Three thin sections were cut from mutually perpendicular planes in each sample (Fig. 3). Section C was cut parallel to the cleavage, section B was cut in the vertical plane perpendicular to C, and section A was cut perpendicular to sections C and B.

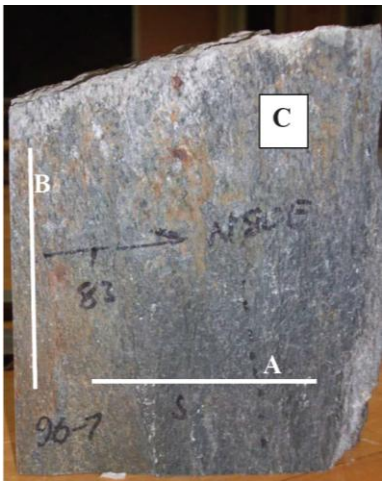

Figure 3. An example of an oriented sample. A, B, and C represent the mutually perpendicular thin sections taken from the sample. Section C was taken parallel to the cleavage, section B was taken in the vertical plane perpendicular to C, and section A was taken perpendicular to sections C and B.

Strain Analysis: The R_f/Φ technique

The R_f/Φ technique (Ramsay, 1967, Dunnet, 1969, Lisle, 1985) allows one to recreate a two-dimensional finite strain ellipse from a planar section in a rock with no initial fabric using objects ("strain markers") that deformed passively, were initially ellipsoidal, and were randomly oriented prior to deformation. The name of the technique, R_f/Φ, refers to the required measurements of each strain marker: the axial ratios (R_f) of each strain marker and orientations of each strain marker's long axis with respect to the direction of maximum extension in the plane of measurement (Φ), or with respect to an arbitrary line (Φ'). R_f and Φ correspond to the undeformed values R_i and θ, respectively (Fig. 4).

Although the measurements are straight forward, different techniques of processing the R_f/Φ data can lead to differences in the interpreted strain ellipsoid (Moriyama and Wallis, 2002). I have chosen to use the θ-curve method, as described by Lisle (1985), because it inherently involves a rigorous statistical analysis to increase the probability of quality data interpretation.

The θ-Curve Method

This is a graphic method of R_f/Φ analysis outlined by Lisle (1985) and explained more concisely by Moriyama and Wallis (2002). If one makes a plot with R_f on one axis and Φ on the other, then strain markers with the same initial orientations (θ), but with different axial ratios (R_f) will define a set of curves on the plot known as θ-curves. The shapes of these curves are determined by the strain ratio (the axial ratio of the strain ellipse = R_s) and are defined by the following equation (Lisle, 1977).

$$Rf = \left[\frac{\tan 2\theta (Rs^2 - \tan^2 \phi) - 2Rs \tan \phi}{\tan 2\theta (1 - Rs^2 \tan^2 \phi) - 2Rs \tan \phi} \right]^{1/2}$$

Each curve radiates from the point $(R_f,\Phi)=(R_s,0)$. The R_s value which best represents the data is determined by comparing sets of θ-curves and determining which set best fits the data. Figure 5 illustrates the relationship between the θ-curves and the deformed clasts.

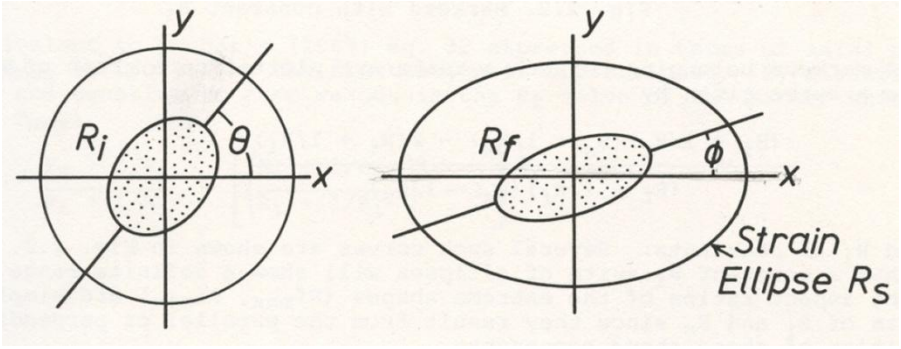

Figure 4. The variables used in R_f/Φ analysis. R_i is the initial axial ratio of the undeformed strain marker in the rock and θ is angle between the long axis of that marker and the line which will become the direction of maximum extension in the strain ellipsoid. R_i and θ correspond to R_f, the axial ratio of the deformed strain marker, and Φ, the angle between the long axis of that marker and the direction of maximum extension in the strain ellipsoid, respectively (Lisle, 1985, figure 2.1).

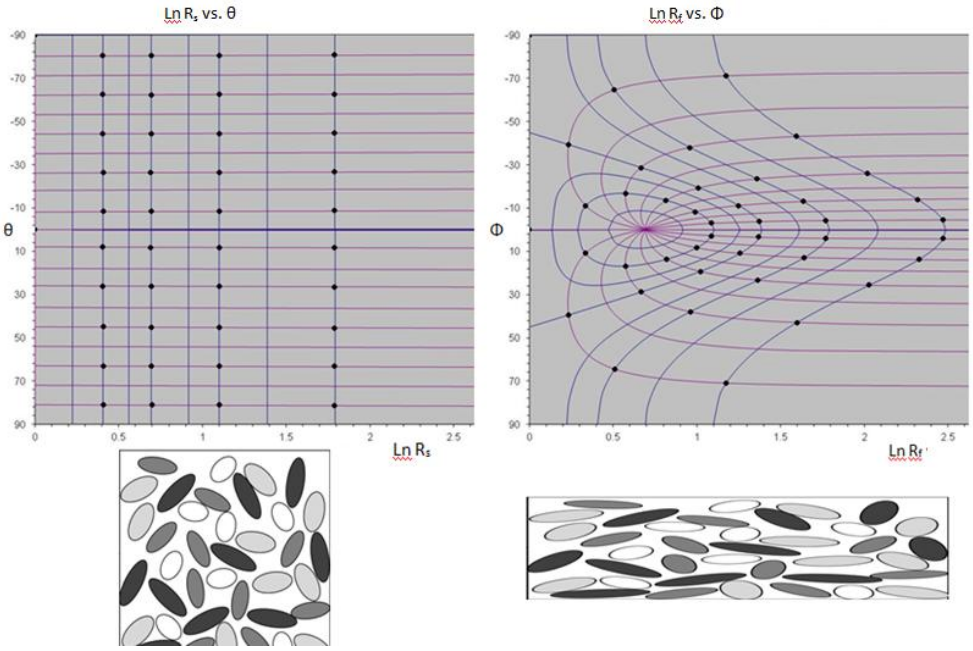

Figure 5. Examples of R_f/Φ plots used in the θ-curve method. All grains are elliptical. Φ is the angular orientation of the long axis of the grains. *Rf* is the axial ratio of the grains. Left: the position of 40 undeformed grains, R_s=0. The horizontal lines are the θ-curves. The vertical lines are contours of the grains initial axial ratios (R_i). Right: the same 40 grains after strain, R_s = 2. The θ-curves all converge at the R_s value.

Determining the best fit is done quantitatively using the χ^2 test (Lisle, 1985). Each set of θ-curves divides the plot into sub-areas and χ^2 is then calculated as:

$$\chi^2 = \sum_{i=1}^{n} (O_i - E)^2 / E$$

where $E = N/n$ (E is the expected number of points plotted to fall within each sub-area, N is the number of strain markers measured, and n is the number of subareas bound by the θ-curves) and O_i is the number of points which fall into each sub-area. The set of θ-curves yielding the lowest χ^2 value is considered the best fit, and the R_s value of that set of curves is the finite strain. For this study an Excel macro developed by D.M. Chew (2002) was used to calculate R_s.

Data Collection

Thin sections of each of the 20 samples were first examined visually to determine whether or not the outlines of the lithic clasts were identifiable through the metamorphic overprint. Approximately 40 lithic clasts were measured from each section of the samples VH96-2, VH96-6, and VH96-8. R_f measurements were made by overlaying a best-fit ellipse on each clast in Adobe Photoshop and recording the length of the axes using arbitrary units. Φ' was measured with reference to the long edge of each thin section, and corrected to Φ automatically by Chew's (2002) Excel macro during analysis by adding the vector mean of Φ', to each Φ' measurement. The vector mean is defined by the following equation.

$$\bar{\phi} = \frac{1}{2} arctan(\Sigma sin2\phi / \Sigma cos2\phi)$$

After the measurements had been gathered and the R_s values determined, a symmetry test was performed as outlined by Lisle (1985) in order to make sure that the clasts were randomly oriented. The test takes the harmonic mean of R_f and the vector mean of Φ and plots them as lines on the R_f/Φ diagram, producing four quadrants. The harmonic mean is defined as:

$$H=\frac{N}{R_{f_1}^{-1}+R_{f_2}^{-1}+R_{f_3}^{-1}...+R_{f_N}^{-1}}$$

where N is the total number of R_f values measured.

The symmetry test is a function of the number of data points that plot in each quadrant and is defined as:

$$I_{sym}=1-\frac{(|n_A-n_B|+|n_C-n_D|)}{N}$$

n_A, n_B, n_C, n_D, are the number of data points that plot in each quadrant. N is the total number of data points.

Possible symmetry-test values range from 0 to 1, with 1 being perfect symmetry. The test values were then compared to "critical values" listed by Lisle (1985), representing a 95% confidence interval that there was no initial fabric in the rock based on the number of strain markers measured and the total finite strain of the rock. For a sample size of 40 clasts, the critical symmetry value is 0.6 for R_s=1.5 and 0.73 for all values above R_s=2 (Lisle 1985). All of the thin sections exceeded symmetry values of 0.73 except for thin section B of sample VH96-6 (symmetry value, 0.51). However, when duplicate points with opposite Φ-values were added to the R_f/Φ plot in order to simulate symmetry, the R_s value only changed by 0.06. Indicating that this low symmetry value is negligible.

The Finite Strain of the Rock

For each sample, the R_s-values from the three mutually perpendicular sections were used to reconstruct the strain ellipsoids. Since the orientation of the strain ellipsoid may not coincide with the orientation of the thin sections, one cannot assume that axes of the strain ellipses from each thin section are the primary axes of strain, unless there is supporting structural evidence. In order to determine the relative lengths of the axes of strain in this study, I assumed that the long and intermediate axes were contained in thin section C which parallels the S_2 cleavage plane (meaning that the direction of maximum stress was normal to S_2). I then determined the relative length of the short axis using the variables explained in figure 5 and the following geometry.

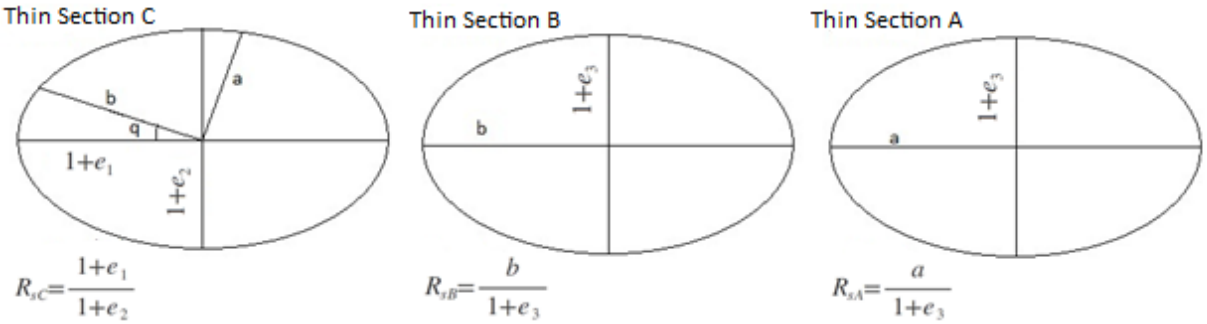

Figure 6. The schematic drawing of the geometric relationship of the axes of the strain ellipses determined from each thin section. R_{sA}, R_{sB}, and R_{sC} are the strain ratios in thin sections A, B, and C, respectively. $1+e_1$, $1+e_2$, and $1+e_3$ are the long, intermediate, and short axes of the strain ellipsoid, respectively. Axis *a* is the long axis of the strain ellipse in thin section A. Axis *b* is the long axis of the strain ellipse in thin section B. Axis *a* is perpendicular to axis *b*. Angle *q* is the angle between *b* and the $1+e_1$ of the strain ellipsoid.

As Ramsay (1967) has shown, for any ellipse there is an invariant value *J* such that:

$$J = \lambda'_i + \lambda'_j \tag{1}$$

where λ'_i and λ'_j are the inverse quadratic elongations, $1/(1+e_i)^2$ and $1/(1+e_j)^2$, of any two perpendicular lines connecting the ellipse with its center. Therefore, looking at thin section C in figure 6, one can say that:

$$\lambda'_1 + \lambda'_2 = \lambda'_a + \lambda'_b \tag{2}$$

where λ'_1, λ'_2, λ'_a, and λ'_b are the inverse squares of $1+e_1$, $1+e_2$, *a*, and *b* respectively. Furthermore, since the R_s values determined by the R_f/Φ technique are ratios, one can assign to $1+e_2$ an arbitrary value of 1, thereby making:

$$R_{sC} = (1+e_1)/(1+e_2) = 1+e_1 \tag{3}$$

and

$$\lambda'_1 + \lambda'_2 = \lambda'_1 + 1 = \lambda'_a + \lambda'_b. \tag{4}$$

One can also use say that since

$$R_{sB}=b/(1+e3) \text{ and}$$
$$R_{sA}=a/(1+e3) \tag{5}$$

that

$$R_{sA}/R_{sB}= a/b \text{ and}$$
$$a= b(R_{sA}/R_{sB}). \tag{6}$$

Substituting equation 6 into equation 4 one gets:

$$\lambda'_1+1=\frac{1}{b^2\left(R_{sA}/R_{sB}\right)^2}+\lambda'_b \tag{7}$$

which, solved for *b* is:

$$b=\sqrt{\frac{\left(\frac{1}{(R_{sA}/R_{sB})^2}+1\right)}{\lambda'_1+1}} \tag{8}$$

After calculating b, one can then solve for $1+e_3$ by rearranging the relationship $R_{sB}= b/(1+e_3)$:

$$1+e_3=b/R_{sB} \quad (9)$$

thereby determining the value of the short axis of the strain ellipse relative to the assigned value of $1+e_2=1$.

The Orientation of the Strain Ellipsoids

After the relative lengths of strain are found, it is necessary to orient the strain ellipsoid in order to compare it to the deformational structures in the rocks. The orientation of $1+e_3$ is assumed to be normal to the cleavage since that is the orientation of maximum stress. Knowing this, only one other axis's orientation is necessary to know the full orientation of the strain ellipsoid. This can be done by finding the angle q between b and $1+e_1$ (Fig. 6).

Φ' was measured with respect to the long side of thin section C, which is parallel to b (see Sample Collection above). By definition, correcting the Φ' angles to Φ means finding the angle between the long side of thin section C and the long axis of strain ($1+e_1$). This was done by finding the vector mean of the Φ' measurements in thin section C (see Data Collection above). Since b and the long side of thin section C are parallel, the vector mean is also the angle between b and $1+e_1$, which is q. Since the S_2 cleavage is vertical, an angle q=0 would indicate a vertical axis.

Results

The results of the strain analysis on the lithic clasts are presented in tables 1 and 2. The R_f/Φ data gathered on quartz grains in samples VH96-6, VH96-7, and VH96-11 by Christensen (2009) were run through the same procedure listed above in order to compare the values with the lithic clasts from this study. Table 1 shows the R_s values for each section of each sample, along with the calculated values of $1+e_1$, $1+e_3$, a, and b. It is worth noting that in sample VH96-7 for the quartz grains, the calculated value of b is larger than $1+e_1$, and the calculated value of a is shorter than $1+e_2$. This is not possible if $1+e_1$ is the long axis of the strain ellipsoid and so this sample is excluded from further discussion.

Table 2 displays the ratios $(1+e_1)/(1+e_2)$ and $(1+e_2)/(1+e_3)$ along with the shape parameter k and the intensity parameter i. The ratios $(1+e_1)/(1+e_2)$ and $(1+e_2)/(1+e_3)$ are used as axes on a plot known as a Flinn diagram, which is used to compare shapes of different ellipsoids (Fig. 7).

The shape parameter k, defines a line that passes through the point (1, 1) and a given point on the Flinn diagram (Fig. 7). It can also be thought of as the slope of that same line. It is calculated by:

$$k=\frac{\left(\frac{1+e_1}{1+e_2}-1\right)}{\left(\frac{1+e_2}{1+e_3}-1\right)}$$

k-values larger than 1 are indicative of constrictive strain. k-values less than 1 are indicative of flattening strain, and k-values approximately equal to 1 are indicative of plane strain.

Table 1. The results of the R_f/Φ analysis. See figure 5 for explanation of the variables. $1+e_1$ and $1+e_3$ are recorded as a relative length to $1+e_2$ which was set equal to unit length to facilitate calculations (see text for explanation). In sample VH96-7, b is longer than $1+e_1$ and a is shorter than $1+e_2$, which is not possible if $1+e_1$ is the long axis of the strain ellipse. This sample is therefore not included in the discussion.

		$1+e_1$	$1+e_2$	$1+e_3$	R_{sA}	R_{sB}	R_{sC}	a	b
Lithic	VH96-2	1.64	1.00	0.53	2.08	2.60	1.64	1.09	1.37
	VH96-6	2.34	1.00	0.54	2.10	2.26	2.34	1.26	1.35
	VH96-8	2.30	1.00	0.71	1.46	2.86	2.30	1.03	2.02
Quartz	VH96-6	1.36	1.00	0.83	1.30	1.46	1.36	1.08	1.21
	VH96-7	1.14	1.00	0.73	1.30	1.66	1.14	0.95	1.22
	VH96-11	1.20	1.00	0.78	1.32	1.50	1.20	1.02	1.16

Table 2. Variables describing the strain ellipsoid measured in each sample. See text for explanation of the variables. VH96-7 for the θ-curve method is not included because of impossible geometry (see table 1 and text).

		$(1+e_2)/(1+e_3)$	$(1+e_1)/(1+e_2)$	k	i
Lithic	VH96-2	1.89	1.64	0.72	1.09
	VH96-6	1.85	2.34	1.57	1.59
	VH96-8	1.41	2.30	3.18	1.36
	avg	1.72	2.09	1.53	1.31
	stdev	0.27	0.39	1.25	0.25
Quartz	VH96-6	1.20	1.36	1.76	0.41
	VH96-7				
	VH96-11	1.28	1.20	0.71	0.35
	avg	1.24	1.28	1.15	0.37
	stdev	0.05	0.11	0.74	0.05

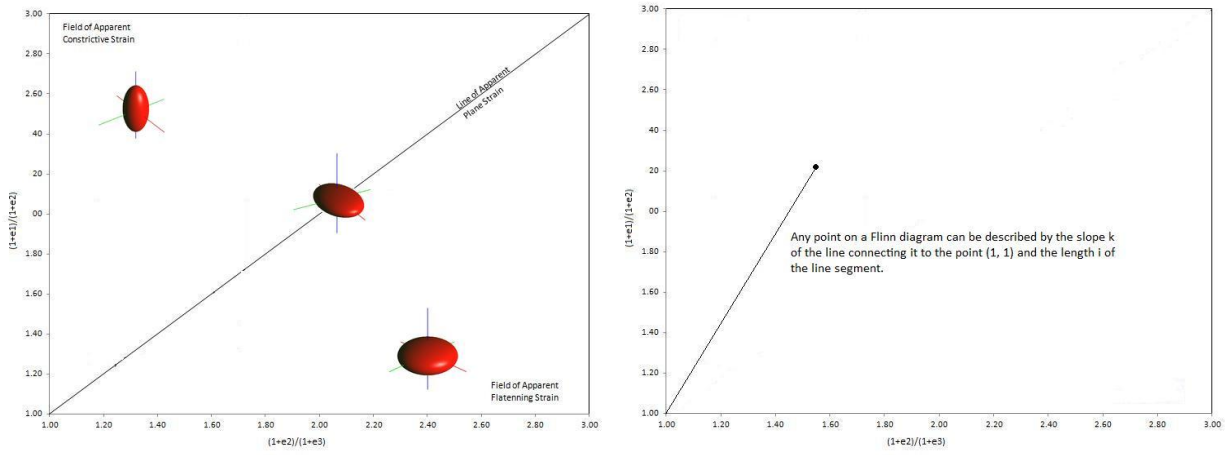

Figure 7. Left: a Flinn Diagram showing how different strain ellipsoids plot. Perfectly biaxial, oblate ellipsoids (pure flattening strain) plot along the horizontal axis. Perfectly biaxial, prolate ellipsoids (pure constrictive strain) plot along the vertical axis. Ellipsoids in which $(1+e_1)/(1+e_2)=(1+e_2)/(1+e_3)$ represent plane strain. Right: Strain ellipsoids can be compared using the quantitative parameters k and i, which describe the slope of the line segment between the point and (1, 1) and the length of the line segment, respectively.

The intensity parameter *i,* represents the distance between the point (1, 1) and a given point on the Flinn diagram (Fig. 7). It can be calculated by the Pythagorean Theorem:

$$i=\sqrt{\left[\left(\frac{1+e_1}{1+e_2}-1\right)^2+\left(\frac{1+e_2}{1+e_3}-1\right)^2\right]}$$

The *i*-value can be thought of as a way to compare the amount of strain from different ellipsoids with similar *k*-values.

Discussion

The average values of the ratios $(1+e_2)/(1+e_3)$ and $(1+e_1)/(1+e_2)$ were plotted on a Flinn Diagram (Fig. 8). The lithic clasts record moderately intense, plane to slightly constrictive strain (axial ratio=2.09:1:0.58, k=1.53, i=1.31); however, larger standard deviations make these values imprecise. The quartz clasts record, more precise, relatively milder plane strain (axial ratio= 1.28:1:0.81, k=1.15, i =0.37). If the two grain types were originally ellipsoidal, randomly oriented, and deformed approximately the same as all other clasts in the rock then they should have recorded the same strain.

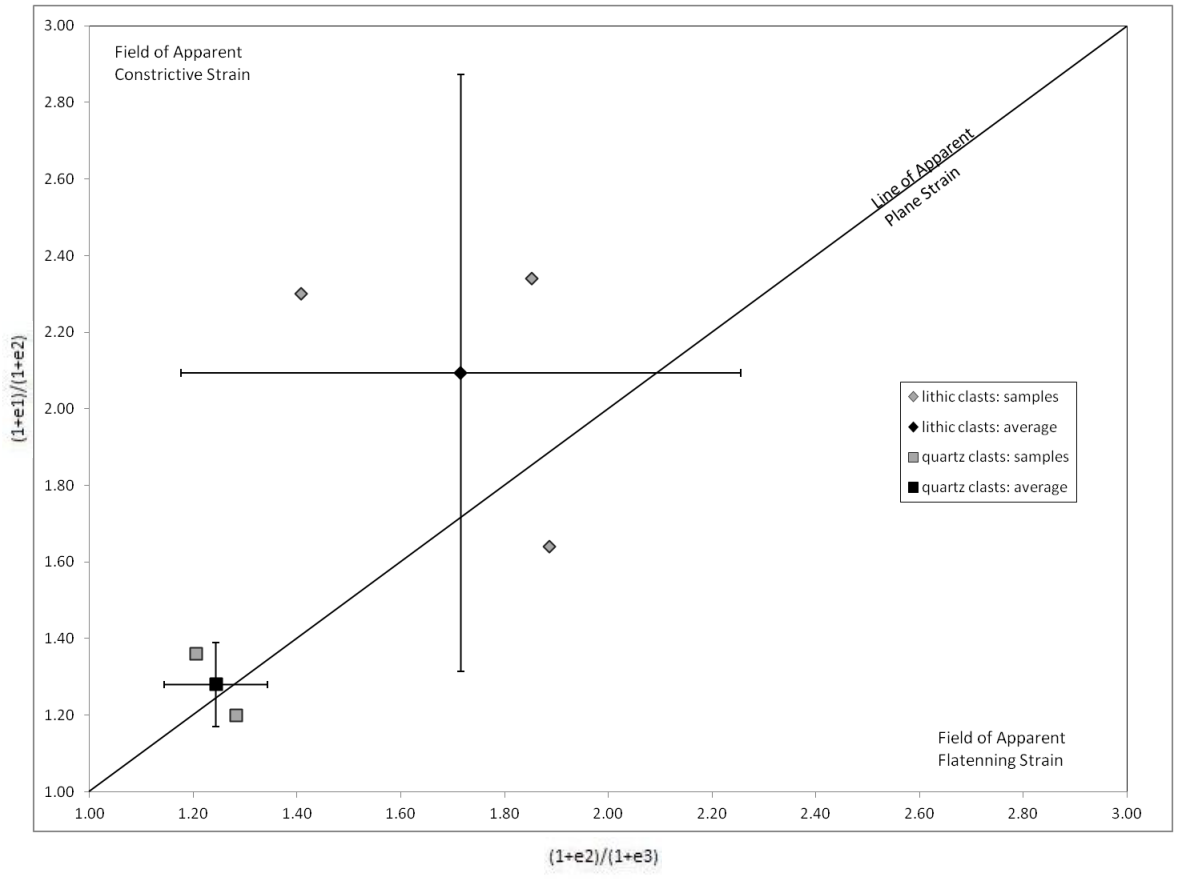

Figure 8. Flinn Diagram displaying average strain ellipsoids determined for each clast type. Error bars are two standard deviations. Lithic clasts: k=1.53, i=1.31. Quartz clasts: k=1.15, i =0.37. See Discussion section for more information.

The discrepancy in measured strain between clast types may be explained by one of the following, or a combination of the following:

1. Small sample size: only three samples of each type were examined and the uncertainties associated with the two clast types overlap. This cannot be investigated without measurements from more samples.
2. A ductility contrast: this would cause the two clast types to deform differently along the same deformation path. In terms of strain parameters, this would mean that the shape parameter *k* should be about the same between the two clast types while the intensity parameter *i* should be greater in one type of clast than the other. The data suggests a ductility contrast does play a role in the discrepancy, with the lithic clasts being more ductile than the quartz clasts, but the uncertainty associated with the *k*- and *i*-values are too large to say so definitively.
3. Grain shape: the R_f/Φ technique requires that strain markers approximate an ellipsoid. A weakness of the R_f/Φ technique is that there are no criteria for exactly how ellipsoidal an object has to be in order to yield accurate strain data. Since the measured clasts were approximately ellipsoidal, one can infer that they were also approximately ellipsoidal prior to deformation; however it is possible that they were not "ellipsoidal enough."

The orientations of long axes of strain were found to be roughly vertical. The values of *q* do not exceed 23 degrees from vertical (Table 3). This strain therefore cannot be associated with D_1 or D_3, because they both involved folding about sub-horizontal axes (Jirsa and Boerboom, 2003). The strain must therefore be primarily from D_2. This matches field evidence of "rare, nearly vertically dipping, tight isoclinal folds" described in the Mud Lake Sequence by Jirsa and Boerboom as D_2 (2003, p 32). A moderately steep D_2 lineation is also present in the higher grade Minntac sequence, lending additional evidence to a shared deformational history between the Mud Lake and Minntac Sequences. This is significant, because the two sequences are only in contact along the Laurentian Fault today, and the original spatial relationship between them is unknown. The shared tectonic history also suggests a relationship between the two sequences' metamorphic history. If this is true, the amphibolites facies of the Minntac Sequence and the prehnite-pumpellyite facies of the Mud Lake Sequence represent different grades of the same metamorphic event.

Table 3. The Vector Mean of Φ' from thin section C for each sample. Vector Mean of Φ' is the same as the angle q in figure 5 and represents angle between the long axis of the strain ellipse and a vertical line. These values are used in orienting the strain ellipse. See text for why sample VH-96-7 for the quartz clasts is excluded.

		Vector Mean of Φ'
Lithic	VH96-2	-22.65
	VH96-6	12.86
	VH96-8	-0.88
Quartz	VH96-6	-18.88
	VH96-11	-9.41

Conclusion

The high symmetry values measured from each sample show that the R_f/Φ strain-analysis technique is reliable in qualitatively determining the strain in clasts from the Mud Lake Sequence. This study suggests that the greywacke-slates of the Mud Lake Sequence underwent mild to moderate plane strain described by *k*-values of 1.15 to 1.69 and *i*-values of 0.37 to 1.41 depending on the type of clast used to measure strain. If a ductility contrast is responsible for the variation in *i*-values between the clast types, additional samples will decrease the range of *k*-values while the *i*-values remain distinct. If there is no ductility contrast between the clast types, then additional data will decrease the range of both *k*- and *i*-values, providing a more precise measurement of finite strain for the whole rock unit.

Although this study did not provide a finite strain value for the Mud Lake Sequence's metasedimentary rocks, it does lead to an improved understanding of the region's deformational history. This study has shown that the long axes of strain in the area are nearly vertical, providing support that D_2 was the primary fabric-producing event. The correlation between the long axes of strain in the Mud Lake Sequence and the moderately steep lineation in the Minntac sequence also helps definitively tie together the deformational history of the two sequences whose original spatial relationship is unknown, because they only lie in fault contact with each other in the modern geologic record.

Works Cited

Chew, D.M., 2003, An Excel spreadsheet for finite strain analysis using the Rf/f technique*: Computers & Geosciences v. 29, no. 6, p. 795-799.

Christensen, B., 2009, Strain analysis of Archean rocks in the Virginia Horn area, NE Minnesota: Undergraduate Thesis, Gustavus Adolphus College.

Dunnet, D., 1969, A technique of finite strain analysis using elliptical particles: Tectonophysics, v. 7, p. 117-136.

Jirsa, M.A., Boerboom, T.J., and Morey, G.B. 1998, Bedrock geologic map of the Virginia Horn Mesabi Iron Range, St. Louis County, Minnesota: Minnesota Geological Survey Miscellaneous Map Series, Map M-85, scale 1:48 000.

Jirsa, M.A., and Boerboom, T.J., 2003, Geology and mineralization of Archean bedrock in the Virginia Horn: Contribution to the geology of the Virginia Horn Area, St. Louis County, Minnesota, Jirsa, M.A., and Morey, G.B. eds., p. 10-73.

Jirsa, M.A., Chandler, V.W., Lively, R.S., 2005, Bedrock geology of the Mesabi Iron Range, Minnesota: Minnesota Geological Survey Miscellaneous Map Series, Map M-163, scale 1:100,000.

Levy, E.R., 1991, The geology andsedimentology of Archean metasedimentary rocks of the Virginia Horn area, northeastern Minnesota: Unpbl. M.S. thesis, University of Minnesota, Duluth.

Lisle, R.J., 1977, Clastic grain shape and orientation in relation to cleavage from the Aberystwyth Grits, Wales: Tectonophysics 39, 381–95.

Lisle, Richard J., 1985, Geological Strain Analysis, A Manual for the Rf/φ Technique: Great Britain, Pergamon Press.

Morey, G.B. Jirsa, M.A., 2003, Overview of the geologic studies in the Virginia Horn area: Contribution to the geology of the Virginia Horn Area, St. Louis County, Minnesota, Jirsa, M.A., and Morey, G.B. eds., p. 1-9.

Moriyama, Y., Wallis, S., 2002, Three-dimensional finite strain analysis in the high-grade part of the Sanbagawa Belt using deformed meta-conglomerate: The Island Arc, 11, p. 111-121.

Ramsay, J.G., 1967, Folding and Fracturing of Rocks, McGraw-Hill, New York.

Welsh, J.L. 1989. Strike-slip faulting in Archean rocks in the Virginia Horn area, N.E. Minnesota: Implications for the origin of the Virginia Horn structure [abs.]: Institute on Lake Superior Geology, 35th Annual Meeting, Duluth, Minn., Proceedings and Abstracts, v. 35, pt. 1, p. 101.

Welsh, J.L, England, D.L., Groves, D.A., Levy, E., 1989, General Geology and the Structure of Archean Rocks of the Virginia Horn Area, Northeastern Minnesota: Institute on Lake Superior Geology Proceedings Part 2: field trip guidebook, v. 35, p. D 1-9.

Welsh, J.L., Englebert, J.A., and Hauck, S.A., 1991, General Geology, Structure, and Geochemistry of Archean Rocks of the Virginia Horn Area, Northeastern Minnesota: Bedrock Geochemistry of Archean Rocks in Northern Minnesota, Center for Applied Reasearch and Technology Development, Natural Resources Research Institute, University of Minnesota, Duluth, Englebert, J.A. and Hauck, S.A eds., p. 100-137.